Cascade structures and scaling exponents in a dynamical model of turbulence: Measurements and comparison

Emmanuel Leveque[1,2] and Zhen-Su She[1,3]
[1]*Department of Mathematics, University of Arizona, Tucson, Arizona 85721*
[2]*Laboratoire de Physique, ENS de Lyon, 69364 Lyon cedex 07, France*
[3]*Department of Mathematics, University of California at Los Angeles, Los Angeles, California 90095*
(Received 16 September 1996)

A detailed examination of the cascade statistics and scaling exponents is carried out for a dynamical-system model of fully developed turbulence called the GOY shell model. The convergence in time of the probability density functions and moments of the velocity fluctuations and their scaling exponents is studied with particular care. With a large sample size (5×10^9), we demonstrate that there exists a finite cutoff for the velocity fluctuations at each inertial-range wave-number shell and the properties of the cutoff determine the scaling exponents of all moments. This cutoff represents the most intermittent structures in the cascade dynamics and exhibits a power-law dependence on wave number. The accurately determined scaling exponents permit a detailed comparison with various phenomenological models describing the statistics of the energy cascade. The consideration of the first and second derivatives of the scaling exponents with respect to the order of the moments p provides the evidence that the hierarchical-structure model [She and Leveque, Phys. Rev. Lett. **72**, 336 (1994)] predicts the best functional dependence on p of the scaling exponents in the GOY shell model. [S1063-651X(97)06403-9]

PACS number(s): 47.27.−i

I. INTRODUCTION

Turbulence is generally described as a dynamical state of a system exhibiting chaotic fluctuations over a wide range of spatial and temporal scales. A customary example is the motion of a fluid at high speed or low viscosity. Of particular theoretical interest is fully developed turbulence at a statistically stationary state where turbulent fluctuations are sustained at all scales, with different mechanisms at different scales. For an ordinary three-dimensional turbulent flow, large-scale fluctuations ($\ell\sim\ell_0$) are usually maintained by an external forcing, or a flow instability, while small-scale fluctuations ($\ell\ll\ell_0$) are sustained by a so-called cascade dynamics which results from the nonlinear interactions (also called the inertial force) between larger eddies. At small viscosity, the cascade dynamics dominate over the viscous damping over a wide range of scales until a characteristic dissipation scale is finally reached ($\ell\sim\eta$). For $\ell<\eta$, fluctuations are then damped out by viscous dissipation, and the flow becomes smooth. When the characteristic forcing and dissipation scales are clearly separated, i.e., $\ell_0\gg\eta$, turbulence then reaches a state of fully developed dynamics. A concise and constructive theoretical understanding of this dynamical state has been stirring up a continuous effort for the last half century.

It is widely accepted that the motion of an ordinary incompressible fluid is accurately described by the Navier-Stokes equations for a wide range of viscosity, or Reynolds number. The Navier-Stokes equations have so been regarded as the first principle for describing turbulence; the turbulent state is identified as the very chaotic solution of the equation. At the present time, rigorous nonlinear analysis of the equation has yielded few constructive results [1,2]. The nature of the difficulty seems to lie in a poor knowledge about the functional space in which a typical turbulent solution evolves. Any *a priori* estimate without taking into account such knowledge does not seem to yield any optimal characterization of the properties of turbulence. Physicists rather investigate these properties from a phenomenological standpoint, that is, starting from hypotheses motivated by experimental and numerical observations. Interestingly, this is also the approach adopted by the mathematician Kolmogorov, according to Yaglom. This line of study has yielded very fruitful results during the past half century and continues to expand nowadays.

While recognizing that eventually the Navier-Stokes turbulence needs to be fully understood, it is worthwhile to examine carefully various other systems exhibiting the essential features of fully developed turbulent dynamics. These features include, from the present phenomenological understanding, the existence of an inertial range of scales where cascade dynamics are fully developed. As one moves away from a deductive approach based on the first principle, such studies are particularly important. Indeed, studies on various turbulent systems allow one to differentiate the Navier-Stokes (NS) system from others and identify the role of the essential ingredients in the NS system: e.g., the conservation laws, the degree of the nonlinearity, etc. More importantly, it may stimulate the development of a general theoretical framework for nonequilibrium systems presenting critical and scale invariance properties. This has been the essential motivation behind the present study of a dynamical-system model of turbulence, namely the GOY shell model.

The GOY shell model is a finite-dimensional dynamical system, first introduced by Gledzer [3] and based on earlier attempts to quantitatively characterize the cascade dynamics

[4,5]. Later, an important extension was made by Ohkitani and Yamada [6] by introducing phase dynamics with complex variables. The dynamics are governed by the following set of ordinary differential equations:

$$\left(\frac{d}{dt}+\nu k_n^2(k_n/k_d)^{\alpha}\right)u_n=f_n+(a_n u_{n+1}^* u_{n+2}^*+b_n u_{n+1}^* u_{n-1}^* + c_n u_{n-1}^* u_{n-2}^*).$$

Here, $\{u_n\}_{0,1,\ldots,N-1}$ is a set of complex variables which model the Fourier space excitations in shells of wave numbers $k_n=k_0\lambda^n \leqslant k < k_{n+1}$, f_n is a driving force usually acting on some low-wave-number shells, e.g., $f_n=f_2\delta_{n,2}+f_3\delta_{n,3}$. The term $\nu k_n^2(k_n/k_d)^{\alpha}u_n$ is a hyperviscosity damping characterized by an exponent α, the kinematic viscosity ν, and the characteristic dissipation wave number k_d determined by the amplitude of ν. At very small ν, the dynamics are essentially inviscid for $k \ll k_d$; the nonlinear couplings make a chain linking the low- and high-wave-number shell fluctuations.

The coefficients of the nonlinear term follow from the requirement that the total kinetic energy $E=\frac{1}{2}\Sigma|u_n|^2$ and the phase volume of this system must be conserved by the inviscid dynamics:

$$a_n=ik_n, \quad b_n=-i\epsilon k_{n-1}, \quad c_n=-i(1-\epsilon)k_{n-2}.$$

Here, both λ (the subsequent scale ratio) and ϵ are free parameters. The nonlinear dynamics also conserves a second dynamical quantity $H=\Sigma E_n/(\epsilon-1)^n$ [7]. For $\lambda=1/(1-\epsilon)$, $H=\Sigma E_n/(\epsilon-1)^n=\Sigma(-\lambda)^n E_n$ and can be identified with the helicity (H_n is an unsigned quantity and $|H_n|\sim k_n E_n$). In the present study $(\lambda,\epsilon)=(2,\frac{1}{2})$, which lies on the energy-helicity conservation curve.

The GOY shell model has received much interest in the last few years. Existing results report that after a transitory regime, the system displays very rich chaotic dynamics, which defines a specific attractor [6,8]. The stationary (invariant) measure on this attractor is not known rigorously, however, many of its properties can be studied numerically. A particular component of this measure, which is of fundamental physical interest, is the (smooth) probability density functions of single-shell variables $|u_n|$. At small viscosity, the system exhibits an inertial range of shells $k_0 \ll k_n \ll k_d$, where such PDF's fully determine the scaling properties of $|u_n|$ through a power-law dependence of the statistical moments $\langle|u_n|^p\rangle$ on the wave number k_n, characterized by some scaling exponents ζ_p:

$$\langle|u_n|^p\rangle \sim k_n^{-\zeta_p}.$$

It is found that the ζ_p's increasingly deviate from Kolmogorov's mean field theory $\zeta_p=p/3$ [9] as p increases, which can be interpreted in terms of some multifractal scaling properties of the fluctuations of the velocity amplitude $|u_n|$ [10,7]. The deviation from Kolmogorov's scalings depends upon the structure of the nonlinear term, i.e., on the particular setting (λ,ϵ) [11]. However, once (λ,ϵ) is fixed such that the energy and the ''helicity'' are conserved, the scaling exponents are found independent of the parameters λ and ϵ [7]. This result suggests that the conservation properties of the nonlinear dynamics play an essential role in determining the inertial-range scalings.

II. MAIN RESULTS

In the present work, we report more careful quantitative studies of the inertial-range statistics. Such a study is necessary in view of testing various theoretical models of the inertial-range describing the energy cascade. Two main problems have affected the quantitative significance of the previous studies. The first problem is related to oscillations of the moments $\langle|u_n|^p\rangle$ across the wave-number shell k_n. These oscillations seem to be due to the discrete nature of the model. This issue has been discussed by Kadanoff *et al.* [7], who then focus on the quantity

$$\Pi_n=(u_{n-1}u_n u_{n+1})^{1/3}.$$

The study of the scaling properties of the moments $\langle|\Pi_n|^p\rangle$ shows that the effect of a major oscillation of period three is reduced and the same scaling laws as $\langle|u_n|^p\rangle$ are observed. In fact, these oscillations have a more complicated structure originating from the rapid falloff of the excitations at the ultraviolet dissipation cutoff k_d. A more accurate determination of the scalings is adopted here and consists in studying the relative scalings: $\langle|\Pi_n|^p\rangle \sim \langle|\Pi_n|^3\rangle^{\zeta_p/\zeta_3}$, a method first used by Benzi *et al.* [12] in measuring scaling exponents in laboratory flows.

The second issue concerns the sample-size effect on the statistical averages. The convergence has never been studied before, although high-order moments have been frequently reported. Note that there exists the same issue for measurements of the scaling exponents in both laboratory experiments and numerical simulations. By working with a large sample size (up to 5 billion), we are able to examine the issue of convergence for moments up to order 20. This allows us to meaningfully discuss the scaling exponents ζ_p of pth-order moments for large p and its derivatives which, as shown later, provides a crucial test for various theoretical models. The calculation of moments are performed by first constructing the probability density functions (PDF's), followed by an integration in the variable of the fluctuating quantities (e.g., $\log_{10}|\Pi_n|$). The exponents are then obtained by an estimation of the local derivative: $\zeta_p/\zeta_3=-d\log\langle|\Pi_n|^p\rangle/d\log\langle|\Pi_n|^3\rangle$. Several schemas are used for such an estimation in order to ensure the robustness of the result. This detailed examination points out the source of uncertainties, leads to some convergence curves, which allows one to extract the values of the exponents, and finally gives an idea about the confidence levels of the results.

With an accurate determination of the scaling exponent ζ_p, we are able to study its functional dependence on p. In particular, with the study of $d\zeta_p/dp$ and $d^2\zeta_p/dp^2$, we are able to evaluate various scaling models of turbulence proposed in the past three decades: the log-normal model [13], the random β model [14], p model [15], the log-stable model [16], and the hierarchical-structure model [17]. This fine comparison shows that the hierarchical-structure model predicts a functional form for ζ_p remarkably close to the measured one. Other models, with optimally chosen parameters,

produce close values for ζ_p at low order, but display an inconsistent tendency for $d\zeta_p/dp$ and $d^2\zeta_p/dp^2$ as p increases.

With a large sample size, up to 5 billion, we demonstrate the existence of a finite cutoff for the velocity fluctuations at each wave-number shell. In other words, the attractor has a compact support. The highest fluctuation events in the inertial-range shells, which will be referred to as the most intermittent structures in the cascade dynamics, show a power-law dependence on the wave number k_n: $|\Pi_n|_{\max} \sim k_n^{-\lambda_\infty}$. The power-law exponent λ_∞ is significantly smaller than the exponents λ_0 of typical fluctuation events $\langle|\Pi_n|\rangle \sim k_n^{-\lambda_0}$, a direct evidence of multiple scaling nature of the cascade dynamics. The existence of the most intermittent structures provides then a solid basis for the hierarchical-structure model of the inertial-range scalings [17].

The reminder of the paper is organized as follows. In Sec. III, we present relevant computational details of the numerical study of the GOY shell model. In Sec. IV, we describe numerical results on the probability density functions of the inertial-range fluctuating quantities, and the convergence study of the moments, specially at high orders. Section V is devoted to the study of the scaling exponents, with a detail assessment of uncertainties and source of errors. In Sec. VI, the measured scaling exponents are compared to various models of the inertial-range energy cascade. This comparison is made more convincing by carrying out a consistent estimate of the first and second derivatives of the scaling exponents $\zeta'(p)$ and $\zeta''(p)$. Finally, Sec. VII is devoted to a discussion of the physical significance of the hierarchical-structure model which, as shown by the results of the above study, stands as the closest phenomenological description of the energy cascade in the GOY shell model.

III. NUMERICAL INTEGRATIONS

The parameters in the numerical integration of the GOY shell model are chosen as follows: The reference wave number $k_0 = 2^{-3}$. Several forcing schemas have been used to investigate the possible dependence of the inertial-range statistics on the forcing mechanism. These schemas include (1) a time-independent forcing acting on a single wave-number shell ($n=3$); (2) a δt-correlated white noise forcing acting on a single wave-number shell ($n=3$); (3) a δt-correlated white-noise forcing acting on two adjacent wave-number shells ($n=2,3$); (4) a random force with a fixed correlation time $\delta t = 2.5\times10^{-4}$ and an amplitude $|f_n| = 0.005\sqrt{2}$ acting on the shells $n=2,3$. The dynamics of the system are therefore deterministic in case (1) and stochastic in the other cases. However, in all cases, the PDF's at the inertial-range scales display the same qualitative and quantitative features, although some discrepancy was expected due to the discrete nature of the shell model. The results presented below have been obtained using the forcing mechanism (4), described above.

We have also investigated the dependence of the inertial range statistics on the value of the viscosity. We did not notice any visible change provided that the viscous cutoff k_d remains located at the same relative position with respect to the discrete shell grids. We have observed oscillations of the global quantities such as the mean dissipation rate as a function of the viscosity which we believe is due to a periodic change of the relative location of k_d as the viscosity decreases. This phenomenon suggests the importance of the dynamics at the viscous cutoff on the whole inertial range, consistent with the results in the hyperviscosity case ($\alpha>0$) [18]. Although we have studied various cases with $N=17$, 22, 27, and 35, the results presented below will focus on the case $N=22$ and $\nu=10^{-7}$. We will refer it to as the standard parameter case.

The system has been integrated forward in time using either a second-order slave-frog Adams-Bashforth scheme [10] or a fourth-order Runge-Kutta scheme. The PDF's obtained using these two different schemas agree accurately. In our present numerical investigation, we have actually chosen the slave-frog Adams-Bashforth scheme, which is more appropriate to resolve the dissipative dynamics. For the standard parameters above, we have set $dt = 2.5\times10^{-4}$. The initial condition is random and arbitrary. The system first ran for approximately 1000–5000 forcing shell turnover times in order to ensure that the system has evolved close to its attractor. Due to the complicated structure of the attractor, there is no absolute criterion to certify that the stationary regime has truly been reached after a finite integration time. We must rely on the convergence of the statistical moments to validate our description of the chaotic attractor.

After the transitory regime, the system reaches a dynamical state in which the characteristic dissipation and forcing shells are clearly separated, leaving an inertial range of shells where an energy cascade towards high-wave-number shells operates at a constant mean rate. For the standard parameter case, the inertial range spreads up to the shell index $n=14-15$, which corresponds to about 10 octaves or 3 decades. The study of the statistical properties of the fluctuations of the velocity amplitude $|u_n|$ in this inertial range is the main subject of the present work.

IV. PDF's AND MOMENTS

The histograms of $\log_{10}|\Pi_n|$ have been constructed from statistical samples collected at each time step along the time evolution of $\Pi_n(t)$. The discretization size of the histograms has been fixed at $\Delta\log_{10}|\Pi_n| = 0.02$ for all n, which realizes a compromise between the requirement to suitably approximate a continuous PDF and to get sufficient regularity (smoothness) in this approximation. With a logarithmic coordinate, one is able to capture the whole structure of the fluctuations of Π_n for both low and high amplitudes. We have independently verified the ergodic property of the GOY shell model by confronting time statistics with mixed ensemble-time statistics. We then found that the ergodicity was remarkably verified. This ensures that the renormalized histograms converge to the PDF's $\mathcal{P}(\log_{10}|\Pi_n|)$, as the number of time samples (proportional to the integration time) increases to infinity.

In Fig. 1, we show the PDF's of $\log_{10}|\Pi_n|$ for two inertial range shells $n=7$ and $n=9$ obtained with various sample size. As seen from Fig. 1, $\mathcal{P}(\log_{10}|\Pi_n|)$ shows a noticeable asymmetry for the left and right tails with a slower decay at the negative values, i.e., for $|\Pi_n|$ close to zero. This asym-

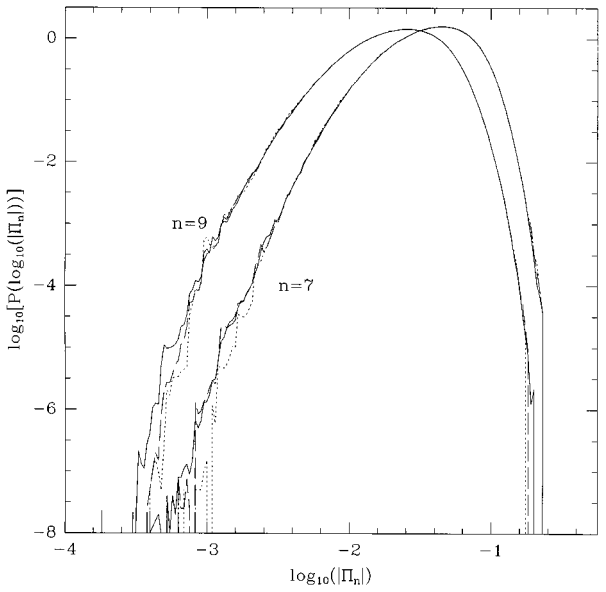

FIG. 1. $\mathcal{P}(\log_{10}|\Pi_n|)$, $n=7,9$ for increasing sample size. Dotted line, 10^9; long-dashed line, 2×10^9; solid line, 5×10^9. Note the convergence of the sharp cutoff at the right tail.

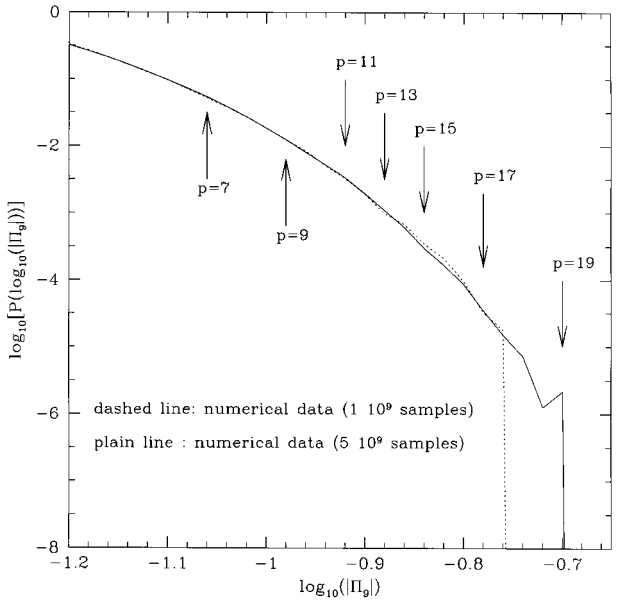

FIG. 2. The magnified tail of $\mathcal{P}(\log_{10}|\Pi_n|)$ for $n=9$.

metry allows us to discover an important property: there exists a maximum for the fluctuation events of Π_n. Indeed, the right tail displays a sharp cutoff at a probability density level much higher (two orders of magnitude at least) than the density level of the cutoff at the left tail which is likely set by undersampling effects. For $n=7$, this maximum value has fully converged for the sample sizes above 1 billon. The convergence appears more slowly for $n=9$; this is natural since stronger and rarer fluctuation events are expected at higher wave-number shells. Note also that the left tail seems to be noisier than the right tail, indicating that the high-amplitude events of Π_n are more coherent, compared to low-amplitude events.

Despite the huge amount of samples collected, the right tail at high-wave-number shells still exhibits fluctuations near the maximum cutoff. This is a consequence of the increasing intermittency at small scales. In Fig. 2, we show a magnification of the large amplitude tail of $\mathcal{P}(\log_{10}|\Pi_n|)$ for two different sample sizes. In Fig. 2, we also indicate the position of the amplitudes where the integrand in the integral of the pth order moment has its peak. When the peak position is close to the ''false'' cutoff, e.g., one obtained for a 1 billon sample size in Fig. 2, we then expect that the evaluation of the high-order moments to be inaccurate. Later results will show that this estimate is roughly correct. On the other hand, if the cutoff is definite, the moment calculation to any arbitrary order should be accurate. Even if the cutoff is not accurately determined, its existence implies a much faster convergence of the high-order moments. Results below will further justify this statement.

In order to obtain a better estimate of the moments, we work with smoothed PDF's. The smoothing does not make any difference for a big sample size ($>10^9$), but makes the convergence faster when the sample size is moderate. This result is suggestive for the treatment of laboratory data which is usually not very large. The smoothing is based on the assumption that the resolution $\Delta\log_{10}|\Pi_n|$ is small enough so that the second derivative of the PDF's can be considered not to change dramatically between nearby bins of $\ln|\Pi_n|$. The technique then smoothes out bumpy fluctuations of the PDF's due to statistical sampling errors. Specifically, we assume that five consecutive points would lie nearly on a second-order parabola whose parameters are then given by a least-squares calculation, which yields

$$\tilde{y}_0 = y_0 - \frac{3}{35}(y_{-2} - 4y_{-1} + 6y_0 - 4y_1 + y_2).$$

The moments are obtained by using the Simpson's rule for the integration schema over the smoothed PDF's. This way, we increase the accuracy of our quadrature formula in the numerical integration of the moments, especially for high-order moments.

Figure 3 shows the relative fluctuation of the moments as a function of the sample size, which is a direct measure of

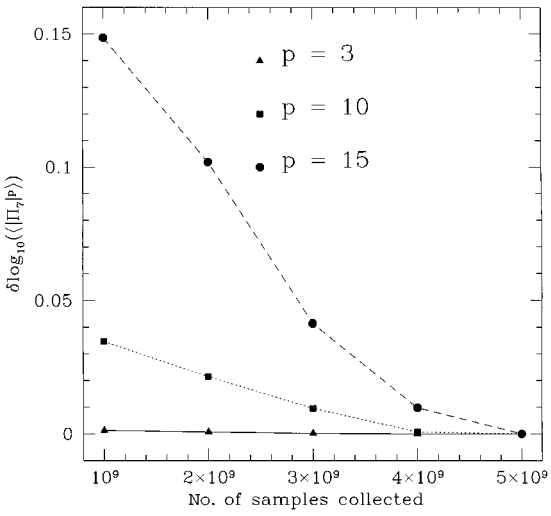

FIG. 3. Convergence of $\langle|\Pi_7|^p\rangle$, $p=5,10,15$.

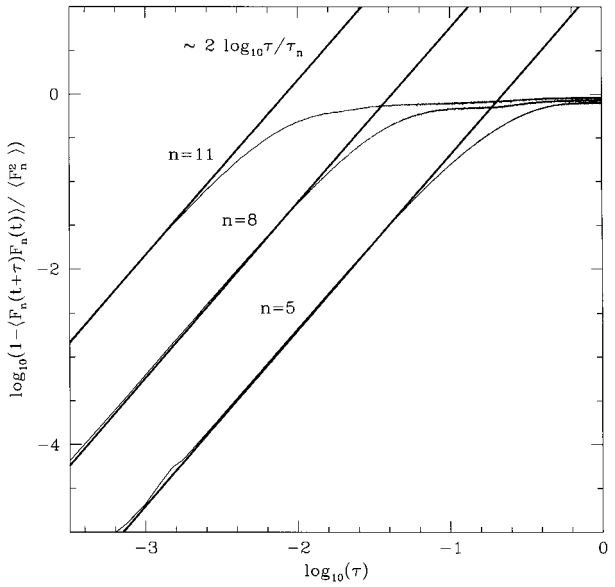

FIG. 4. Two-point time correlation functions of the energy flux.

the convergence. The fluctuations of the moments here are relative to the asymptotic value obtained with a 5×10^9 sample size. This representation enables a synthetic view of the convergence of the moments at different orders. The second-order moments have practically fully converged for sample sizes above 10^9. At the sample size 4×10^9, all moments up to the order 15 are within a 1% margin. Keeping these results in mind will be useful in judging the source of the uncertainty in the determination of the scaling exponents.

For practical purposes, it is important to formulate the convergence results in terms of the length of the time signal in a dynamical time unity, which is more related to the number of independent samples. The natural dynamical time scale at a particular wave-number shell corresponds to the local turnover time or correlation time, which can be estimated from the two-point time correlation functions. In Fig. 4, we present the two-point correlation functions $\langle F_n(t)F_n(t+\tau)\rangle$ of the energy flux at different inertial-range shells. For small τ, $\langle F_n(t)F_n(t+\tau)\rangle=\langle F_n^2(t)\rangle(1-\tau^2/\tau_n^2)$. We then define τ_n as the time unit which plays a similar role as the Taylor microscale in Navier-Stokes turbulence. Figure 5 shows the variation of τ_n as the wave number k_n. In the log-log plot, it shows that the variation over the inertial-range wave-number shells exhibits closely a power-law behavior.

Using τ_n as a measure of the time unity, we have examined the convergence of the moments at various wave-number shells. A typical result is shown in Fig. 6, where the relative convergence of the 10th-order moment is examined. It can be seen that the present time signal used in order to construct these statistics is very long in terms of the dynamical correlation time unity; of the order of 10^6 to 10^8. It appears that the moments at high-wave-number shells converge more slowly, even though they have a bigger effective sample size due to a smaller dynamical turnover time. This can be explained by the fact that dynamics are more intermittent at higher-wave-number shells; high amplitude events are captured in a more irregular and disordered way. The high amplitude tail is then more bumpy and requires a lot

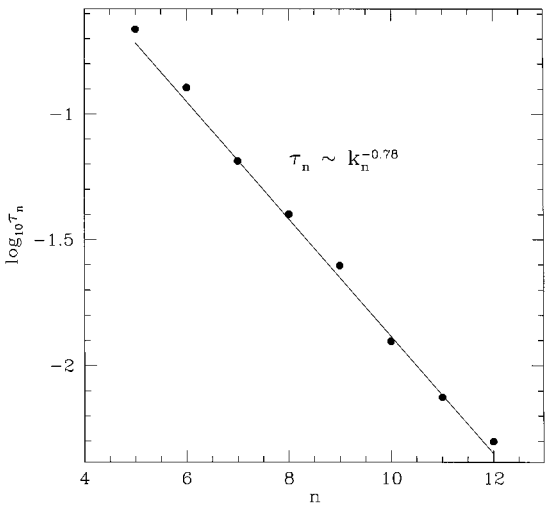

FIG. 5. Correlation time as a dynamical time unity, as function of $\log_2 k_n/k_0=n$.

more statistical events to converge to its asymptotic shape. This naturally slows down the convergence of high-order moments at high wave numbers.

V. SCALING EXPONENTS

The above results establish that the moments only fluctuate within 1% up to the order of 15 (and just a few percent up to the order of 20) for a sample size from 1×10^9 to 5×10^9. If the moments behave exactly in power law with the wave number k_n, the exponents can then be derived from the local derivative:

$$\zeta_p=-\frac{d\log\langle|\Pi_n|^p\rangle}{d\log k_n}.$$

The existence of a scaling range is then manifested by the constancy of the local derivative over a finite range of wave numbers. Our estimation of the scaling exponents below will be based on the evaluation of the local derivative and on its constancy property.

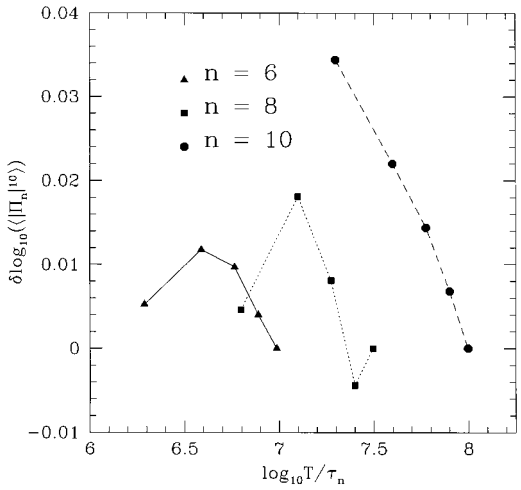

FIG. 6. Convergence of $\langle|\Pi_n|^{10}\rangle$, $n=6,8,10$ in dynamical correlation time unit.

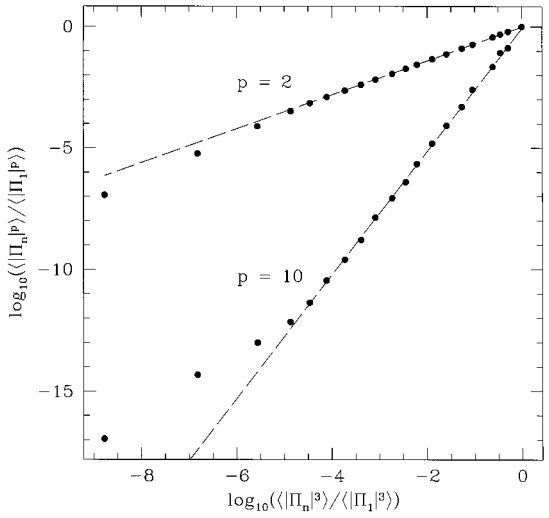

FIG. 7. Relative dependence of the moments showing clear relative scalings.

In the shell model, however, we have a discrete set of k_n so that the derivative cannot be accurately evaluated by a low order finite difference approximation. More seriously, $\log_{10}\langle|\Pi_n|^p\rangle$ exhibits oscillatory behavior with respect to the shell index n, even when the product of three adjacent shells (Π_n) is considered. Such an oscillation jeopardizes considerably the locale derivative calculation. In order to make a reasonable estimate, we choose to consider the so-called relative scaling exponents, that is,

$$\zeta_p/\zeta_3=\frac{d\log\langle|\Pi_n|^p\rangle}{d\log\langle|\Pi_n|^3\rangle}.$$

The relative scaling exponents are much less sensitive to ''global'' oscillations through wave-number shells, and give a better characterization of the change of shape of the PDF's with n. Measuring the relative scaling exponents was first suggested by Benzi *et al.* [12] who refer it to as an extended self-similarity (ESS) property of the statistical moments. Indeed, they showed that, when plotting $\log_{10}\langle|\delta v_{/}|^p\rangle$ against $\log_{10}\langle|\delta v_{/}|^3\rangle$ for the experimental data of the velocity structure functions, a more extended range of the inertial-range scaling is observed. This property can be interpreted as follows: As the viscous range is approached, a variation of some global parameters in the PDF's is introduced, which does not affect the characteristic deformation of the PDF's due to the nonlinear cascade dynamics, so that a longer power-law range is obtained for the relative moments. In the shell model, the oscillations due to the discreteness are also related to the variation in shells of some global parameters in the PDF's, relatively distinct from the deformation due to the nonlinear cascade dynamics, so that we expect to see better relative scaling behavior. Note that because $\zeta_3\equiv 1$ theoretically, the relative scaling exponents defined above in the inertial range are equal to the absolute scaling exponents.

In Fig. 7, we display the relative dependence of $\langle|\Pi_n|^p\rangle$ on $\langle|\Pi_n|^3\rangle$ for $p=2,10$ over wave-number shells. In the log-log plot, a clear scaling range is displayed. The lines have the slope which we obtained from a ''mean'' estimate of the local derivatives, as we explain now. We have used several

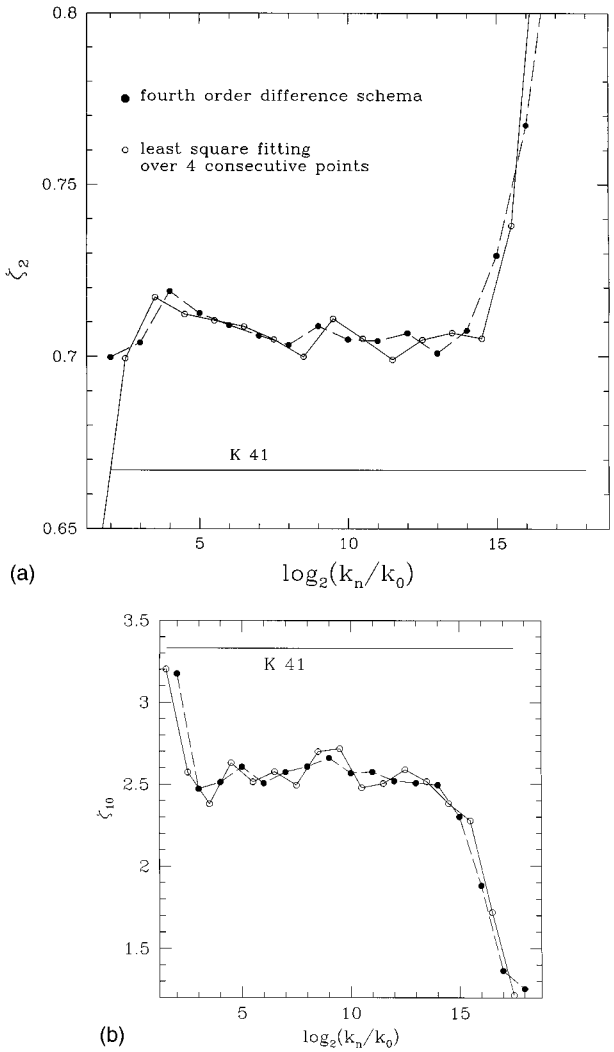

FIG. 8. (a) Local derivative estimated for the second-order moments. (b) Local derivative estimated for the tenth-order moments.

different approximations for evaluating the local derivatives, in order to ensure the robustness of the results. The best two methods are a least-squares fit by a straight line using four adjacent points and a fourth-order difference schema using five adjacent points. The results are shown in Fig. 8(a) and Fig. 8(b). We may see the existence of a range (from the wave-number shells 5–14) where the local derivatives are roughly constant, although ocsillations are still persistent. Remarkably, the local derivatives oscillate around values clearly distinct from the Kolmogorov scalings [9] for both $p=2$ and $p=10$. The two approximation schemas show qualitatively the same and quantitatively close behavior of the local derivative. We then regard these local derivatives as the local scaling exponents.

At this point, it is important to check the convergence of the local scaling exponent estimate as a function of the sample size, since errors of several percents occur for moments of order larger than 10. In Fig. 9, we display the ratio of the local scaling exponents estimate at several sample sizes to the final derivative values obtained at the sample size of 5×10^9. The result shows that from 3 to 5 billion sample sizes, the local scaling exponents differ by only 0.5%, much smaller than the scattering due to the oscillations across

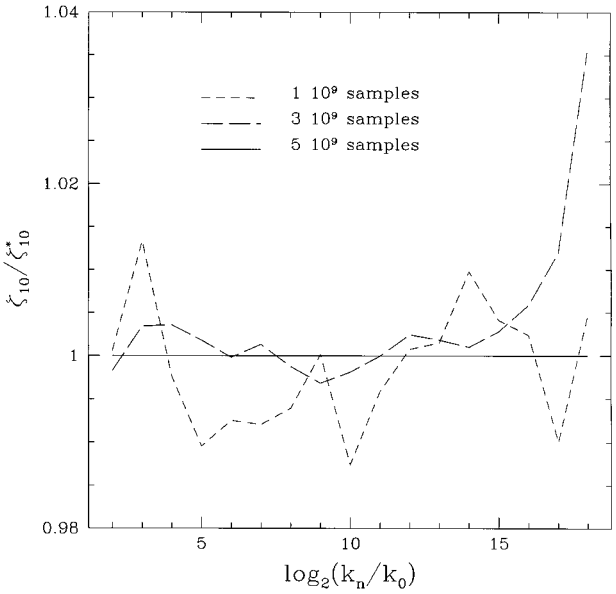

FIG. 9. Convergence check of the local derivative estimate.

wave-number shells. It is also interesting to note that the convergence is faster for the local scaling exponents than for the moments which, according to Fig. 3, differ by 1% at 3 billion sample size. This can be interpreted by the fact that adjacent wave-number shells have some common deficiency in the estimation of the moments which, when the local derivative is evaluated, partially cancel as a systematic error, yielding a more accurate estimate of the scaling exponents. We believe that this is the reason why even with very insufficient sample size, experimental data still give a reliable indication of the anomalous scalings in turbulence.

A more quantitative estimate of the convergence rate of ζ_p is shown in Fig. 10. For a dynamical turnover time of 5×10^6 and 2×10^7, ζ_5 does not show any fluctuations, ζ_{10} shows some 0.5% and ζ_{15} some 1.5% fluctuations. This convergence curve in terms of the dynamical turnover time is useful in accessing the possible convergence of experimental measurements. In a typical experimental data collection, it is

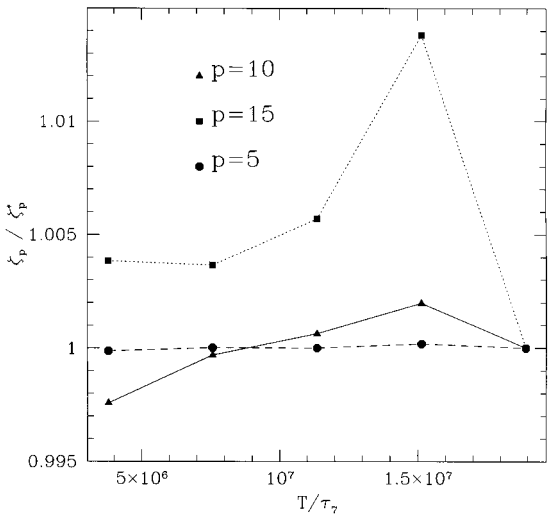

FIG. 10. Convergence of ζ_p in dynamical correlation time unit.

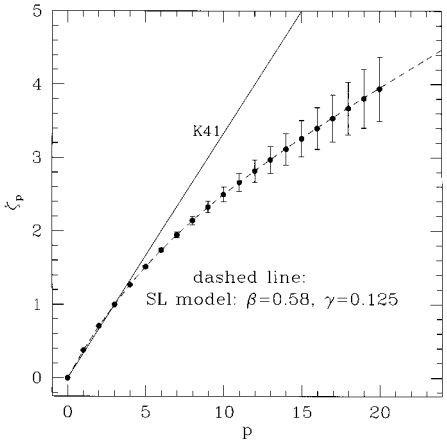

FIG. 11. The ''mean'' estimate of the anomalous scaling exponents.

hard to go above 10^6 dynamical turnover time. Therefore, the result presented here represents the best estimate to attain.

The scaling exponents ζ_p obtained from the average over the wave-number shells from 5 to 14 is plotted in Fig. 11. The present study allows one to a clear identification of two kinds of errors: (1) errors due to discrete dynamics, and (2) errors due to insufficient statistics. The second kind of error is made very small due to the large sample size, while the first kind intrinsic to the model remains the principle source of uncertainty. The final error is obtained by estimating the scattering due to the oscillations in Fig. 8. Since oscillations are primarily caused by the discreteness of the model, it seems impossible to improve our estimates even with more statistical samples. Clearly, the error estimate is conservative. Note that with more realistic dynamics free of discrete oscillations such as in the 3D Navier-Stokes turbulence simulations or in laboratory measurements with adequate resolutions, the exponents should be determined with higher accuracy.

Nevertheless, anomalous scaling exponents are clearly evidenced beyond any doubt. In Fig. 11, we present the exponents ζ_p with the error estimate from the oscillations. The line in Fig. 11 is a fit of the hierarchical-structure model which has been recently proposed by us. In Table I, we report also the numerical values of the exponents. The mean values of the shell-model scalings are all within 0.5% close to the values of the theoretical model. The agreement between the theoretical ζ_p and the numerically measured ζ_p is truly remarkable. Note that the parameters in the hierarchical-structure model can be directly obtained from the ζ_p measured; the fitting is then straightforward (see the next section). The success of the hierarchical-structure model is more apparent by a detailed comparison with other proposed energy cascade models in the next section. Such a remarkable agreement should not be accidental. We will discuss its physical significance in Sec. VII.

VI. COMPARISON TO THEORETICAL MODELS

The purpose of performing such a detailed study of the scaling exponents is to test various models of the energy cascade of fully developed turbulence. As discussed in the Introduction, all phenomenological models of the energy

TABLE I. Comparison of the scaling exponents ζ_p measured in numerical simulations of the GOY shell model with the hierarchical-structure model [17] in which the parameters are suitably chosen.

Order p	ζ_p/ζ_3 (shell model)	SL model: $0.125p+1.49(1-0.58^{p/3})$
1	0.375±0.005	0.372
2	0.705±0.003	0.703
3	1.000	1.000
4	1.268±0.006	1.268
5	1.512±0.014	1.513
6	1.738±0.026	1.737
7	1.946±0.040	1.946
8	2.141±0.058	2.140
9	2.323±0.078	2.323
10	2.50±0.10	2.50
11	2.66±0.13	2.66
12	2.82±0.15	2.82
13	2.97±0.18	2.97
14	3.12±0.21	3.12
15	3.26±0.25	3.27
16	3.40±0.28	3.41
17	3.54±0.32	3.55
18	3.67±0.36	3.68
19	3.80±0.40	3.82
20	3.94±0.44	3.95

cascade make no direct link to the Navier-Stokes equations; therefore, they should also apply to the GOY shell model. Despite the discreteness, the shell model presents remarkable cascade dynamics, and exhibits anomalous scaling laws which merit a quantitative theoretical description predicting a correct form of ζ_p. In this section, we make a detailed comparison with some existing models.

The models confronted in this comparison include (1) the log-normal model [13] $\zeta_p=p/3+(\mu/18)(3p-p^2)$; (2) the random-$\beta$ model [14]: $\zeta_p=p/3-\log_2(1-x+x2^{p/3-1})$; (3) the p model [15]: $\zeta_p=p/3-\mu(p/3)^\alpha-(p/3)/(2^\alpha-2)$; (4) the log-stable model: $\zeta_p=p/3+1-\log_2[\lambda^{p/3}+(2-\lambda)^{p/3}]$ [16]; (5) the She-Leveque model: $\zeta_p=\gamma p+(1-3\gamma)(1-\beta^{p/3})/(1-\beta)$ [17]. In Fig. 12, we compare ζ_p with all the models above with parameters chosen in such a way as to minimize deviation to the numerical ζ_p at small p (for the log-stable model, we use the parameter values suggested by Kida [16]). We also plot the exponents of the present numerical computation with increasing sample size to give an idea about the numerical convergence of the scaling exponents. It can be seen that the p model and She-Leveque model give a satisfactory description over most of the range of p. Although the other three models give the exponents values close to the numerical ones over some range of p, a sharp glance at the figure indicates some inconsistency for large p. In order to allow a more accurate differentiation among the models, we propose to study $d\zeta_p/dp$ and $d^2\zeta_p/dp^2$, which gives a much better characterization of the variation of ζ_p on p.

The evaluation of the numerical $d\zeta_p/dp$ and $d^2\zeta_p/dp^2$ have to rely again on some finite difference approximation. From the PDF's, we can compute moments of all orders

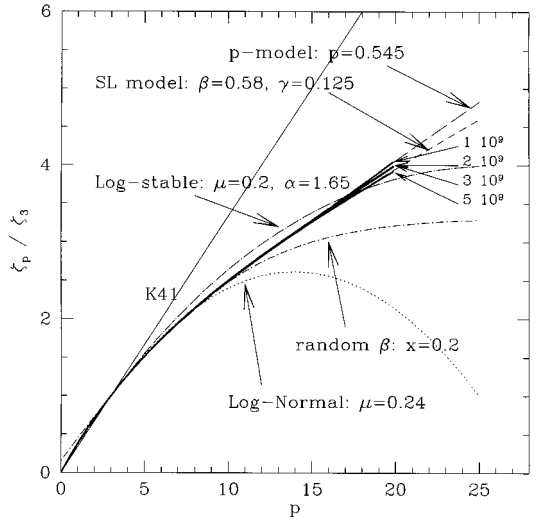

FIG. 12. Scaling exponents ζ_p compared to various models.

including moments of fractional orders. The question that may arise is that since each exponent is obtained with a certain level of accuracy (i.e., finite number of significant figures), does it make sense to perform a finite difference calculation? We believe that it is possible provided that a local exponent estimated at some fixed point is consistently used in the evaluation. The argument is that for an infinitesimal change of the order p, most errors are common to different orders so that they finally cancel. The relative error of the derivative is of the same order as the exponent itself. We have decided to study $d\zeta_p/dp$ and $d^2\zeta_p/dp^2$ from the local exponent ζ_p obtained at a fixed wave-number shell ($n=7$) and indeed we obtained a smooth curve for the both derivatives. The first derivative is obtained with a fourth-order interpolation formula:

$$f'(x_0)\approx\frac{-2f(x_{-2})-f(x_{-1})+f(x_1)+2f(x_2)}{10h},$$

where h is the equidistant interval between x_n and x_{n+1}, and the second derivative with the following interpolation formula:

$$f''(x_0)\approx\frac{1}{100h^2}\{9f(x_{-3})+6f(x_{-2})-5f(x_{-1})-20f(x_0)$$
$$-5f(x_1)+6f(x_2)+9f(x_3)\},$$

The results are presented in Fig. 13 and Fig. 14, at several sample sizes. It is no surprise that the convergence is slower for derivatives, but the tendency of the curve is quite clear.

It is quite remarkable that $\log_{10}|d^2\zeta_p/dp^2|$ derived from the numerical computation data tends to a straight line as the sample size increases, as predicted by the hierarchical-structure model. No other model predicts this tendency. It is interesting to note that from Fig. 14, we can derive the values of the two parameters in the hierarchical-structure model, β and γ, which are related to the slope of the line and its intercept with the vertical axis. This property makes the determination of the parameters very straightforward. As shown by Dubrulle [19] and She and Waymire [20], the ex-

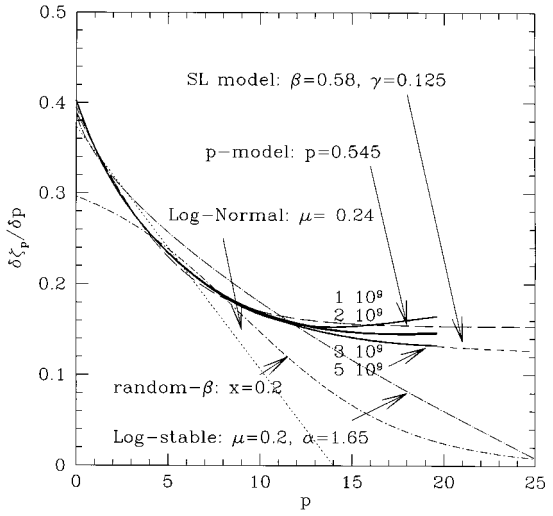

FIG. 13. First derivative of scaling exponents $d\zeta_p/dp$ compared to various models.

istence of a hierarchy of structures can be exactly realized by a random multiplicative process with log-Poisson statistics. The present numerical evidence then suggests the log-Poisson process as the closest description of the cascade dynamics of the GOY shell model. While a mathematical proof is still lacking, the physical significance of this result is worth being explored. We address this issue in the next section.

VII. DISCUSSIONS: THE HIERARCHICAL STRUCTURES OF THE ENERGY CASCADE

The basic phenomenology in the hierarchical-structure model [17] is that the cascade events do not fluctuate up to any arbitrary amplitude, but up to some maximum value. In other words, the trajectories of the asymptotic long-time dynamics of the system evolves in a bounded domain in the phase space, and therefore the PDF of the fluctuations (e.g., Π_n) at each wave-number shell has a compact support. The upper bound in the velocity fluctuations at each wave-number shell represents the largest, or the most intermittent, fluctuation event. Intuitively, these structures should play a role in controlling the dynamics. We are then motivated to look for direct evidence of the existence of such most intermittent structures. In Fig. 15, we display the relative variation of $\log_{10}|\Pi_n|_{\max}$ for a series of shells in the inertial range ($n=6,8,10$). Clearly, the maximum amplitude events for $n=6,8$ have converged in each shell after 2 billion samples have been collected, whereas for $n=10$ some increase occurs between 4 and 5 billon samples. A slower convergence of the amplitude of the maximum events at larger wave-number shells is consistent with an intermittent cascade.

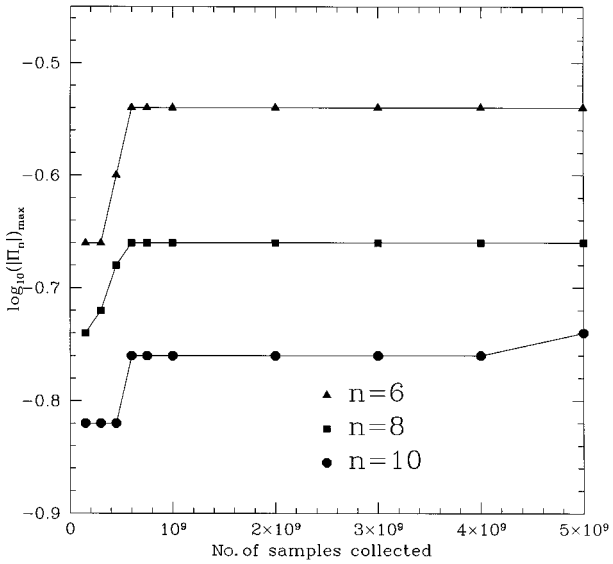

FIG. 15. Convergence of $\log_{10}(|\Pi_n|)_{\max}$ for $n=6,8,10$.

One remarkable property of the most intermittent cascade event is its dependence on the wave number. In Fig. 16, we show the relative dependence of the maximum fluctuation event on the third-order moments, from which we derive an approximate scaling exponent -0.16. In the hierarchical-structure model [17], this exponent corresponds to the parameter λ_∞. Here, it is smaller than the parameter $\lambda_\infty=-0.125$ used in the fitting of the scaling exponents

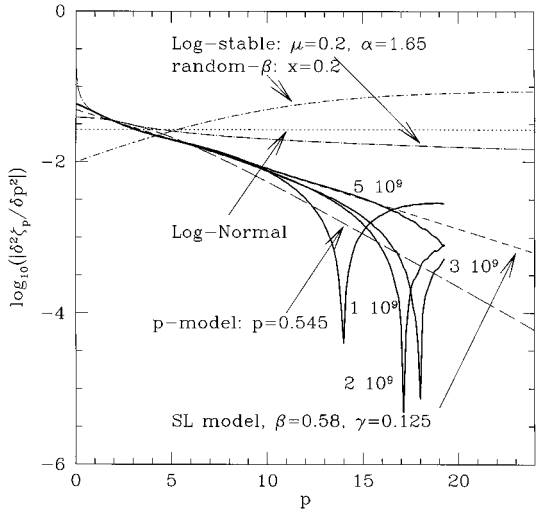

FIG. 14. Second derivative of scaling exponents $d^2\zeta_p/dp^2$ compared to various models.

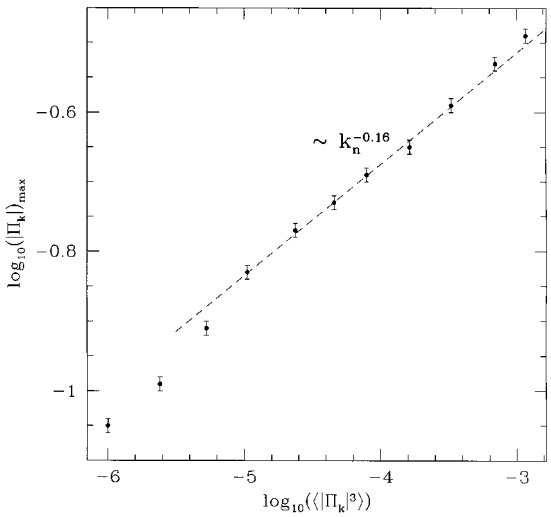

FIG. 16. Scaling behavior of $\log_{10}(|\Pi_n|)_{\max}$.

(Figs. 11–14); this may be due to the fact that the maximum values at higher wave number shells have not fully converged. Indeed, an increase in their values would make the line flatter in Fig. 16.

The fact that the maximum fluctuation event displays a scaling different from that for the typical fluctuation events ($\langle \log_{10}|\Pi_n|\rangle \sim k_n^{-0.37}$) shows that the cascade dynamics in the shell model have multiscaling properties. The question we had raised previously, and which actually leads to the proposal of the hierarchical-structure model, is whether there is any relation between the exponents of the most intense events and the typical intensity events. The key idea in the hierarchical-structure model is that both events, and in fact all events in between, should be related because of the dynamical constraint expressed through the equation of motion. In addition, a certain kind of similarity law should underly such a relation. This motivates the proposal that

$$\Pi_n^{(p+1)} = A_p \Pi_n^{(p)\beta^{1/3}} \Pi_n^{(\infty)1-\beta^{1/3}},$$

where $\Pi_n^{(p)} = \langle |\Pi_n|^{p+1}\rangle / \langle |\Pi_n|^p \rangle$ stands for the pth order fluctuation events and A_p is a constant independent of the shell index n.

For the PDF's we consider here, $|\Pi_n|^{(p)}$ monotonically increases with p and therefore represents a hierarchy of amplitude levels of the velocity fluctuations. The above relation means that if two events of different order (or different amplitude) display different scalings, every other amplitude event will scale in a way which can be determined self-similarly. In order to specifically verify the above self-similarity structure of the hierarchy $|\Pi_n|^{(p)}$, we plot in Fig. 17 $\log_{10}|\Pi_n|^{(p+1)}$ as a function of $\log_{10}|\Pi_n|^{(p)}/|\Pi_n|^{(1)}$ for different levels $p=1,\ldots,15$ at different inertial range shells $n=6,\ldots,9$. The parallel lines observed provide the evidence that the symmetry relation proposed above is accurately satisfied by the hierarchy of the fluctuation levels $|\Pi_n|^{(p)}$. Futhermore, the constants A_p are independent of p; similar results have been obtained by Ruiz-Chavarria *et al.* [21] from laboratory turbulence data. The relation which relates the different fluctuation levels of the hierarchy is therefore not only independent of the shell index n but also independent of the order p of the levels concerned. Note finally that the slope of the parallel lines in Fig. 17 provides a new measurement of the parameter β, fully consistent with the previous estimation, i.e., $\beta=0.58$.

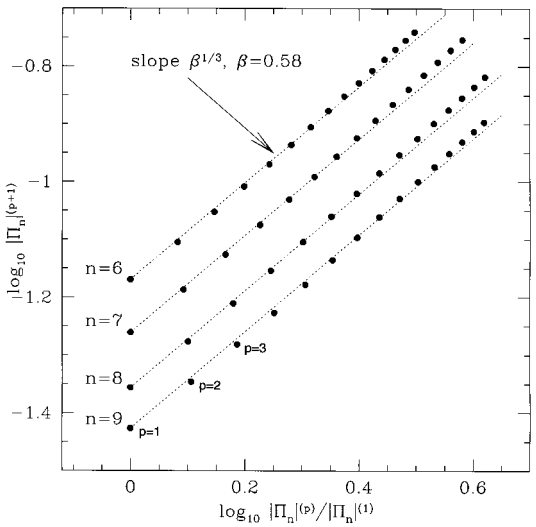

FIG. 17. Evidence of the scaling hierarchy.

In summary, the numerical results presented in this paper unambiguously demonstrate the existence of anomalous (non-Kolmogorov) scaling exponents characterizing the cascade dynamics of the shell model; in particular, the scaling exponent of the kinetic energy definitely deviates from the 2/3 law, despite the numerical uncertainty due to the oscillations introduced by the discrete shell dynamics. Further study of the derivative of the local scaling exponent with respect to the order ($d\zeta_p/dp$ and $d^2\zeta_p/dp^2$) gives more detailed information about the functional form of the exponents ζ_p, which allows one to test various theoretical models of the energy cascade. It is fair to conclude that the hierarchical structure model recently proposed by us (She-Leveque model) gives the closest description of the cascade dynamics and structures.

ACKNOWLEDGMENTS

This work was supported by the Office of Naval Research under Contract No. N00014-9510444. Z.S.S. gratefully acknowledges support from the Alfred P. Sloan Foundation.

[1] R. Temam, *Navier-Stokes Equations: Theory and Numerical Analysis* (North-Holland, Amsterdam, 1984).
[2] P. Constantin and C. Foias, *Navier-Stokes Equations* (The University of Chicago Press, Chicago, 1988).
[3] E. B. Gledzer, Sov. Phys. Dokl. **18**, 216 (1973).
[4] A.M. Obukhov, Atmos. Oceanic Phys. **7**, 41 (1971).
[5] V.N. Desnyanski and E.A. Novikov, Izv. Akad. Nauk. SSSR Fiz. Atmos. Okeana **10**, 127 (1974).
[6] M. Yamada and K. Ohkitani, J. Phys. Soc. Jpn. **56**, 4210 (1987); Prog. Theor. Phys. **81**, 329 (1989).
[7] L. Kadanoff, D. Lohse, J. Wang, and R. Benzi, Phys. Fluids **7**, 617 (1995).
[8] M.H. Jensen, G. Paladin, and A. Vulpiani, Phys. Rev. **A 43**, 798 (1991).
[9] A.N. Kolmogorov, C. R. Acad. Sci. URSS **30**, 301 (1941).
[10] D. Pisarenko, L. Biferale, D. Courvoisier, U. Frisch, and M. Vergassola, Phys. Fluid A **5**, 2533 (1993).
[11] P. Frick, B. Dubrulle, and A. Babiano, Phys. Rev. E (to be published).
[12] R. Benzi, S. Ciliberto, C. Baudet, F. Massaioli, R. Tripiccione, and S. Succi, Phy. Rev. E **48**, R29 (1993).
[13] A.N. Kolmogorov, J. Fluid Mech. **13**, 82 (1962).
[14] R. Benzi, G. Paladin, G. Parisi, and A. Vulpiani, J. Phys. A **17**, 3521 (1984).

[15] C. Meneveau and K.R. Sreenivasan, Phys. Rev. Lett. **59**, 1424 (1987).
[16] S. Kida, J. Phys. Soc. Jpn. **60**, 5 (1990).
[17] Z.-S. She and E. Leveque, Phys. Rev. Lett. **72**, 336 (1994).
[18] E. Leveque and Z.-S. She, Phys. Rev. Lett. **75**, 2690 (1995).
[19] B. Dubrulle, Phys. Rev. Lett. **73**, 959 (1994).
[20] Z.-S. She and E.C. Waymire, Phys. Rev. Lett. **74**, 262 (1995).
[21] G. Ruiz-Chavarria, C. Baudet, and S. Ciliberto, Phys. Rev. Lett. **74**, 1986 (1995).